*Clay Minerals* (2022), **57**, 131–138
doi:10.1180/clm.2022.21

CAMBRIDGE UNIVERSITY PRESS

**Article**

# A molecular dynamics study of the mechanical properties of kaolinite under uniaxial and isothermal compression at various temperatures

Y. Cui[1], H. Y. Wang[2], H. Y. Zhao[1] and H. Yang[3]*

[1]The Third Construction Engineering Company Ltd of China Construction Second Engineering Bureau, Beijing 100070, China; [2]China Mobile Communications Group Company LTD., Beijing 100032, China and [3]School of Aeronautics and Astronautics, Zhejiang University, Hangzhou 310027, China

**Abstract**

Uniaxial and isothermal compression tests of kaolinite were carried out using molecular dynamics simulations. Five different temperatures (300, 400, 500, 600 and 700 K) and pressures ranging from 0.0001 to 50 GPa were selected to study the temperature and pressure effects on the mechanical properties of kaolinite. As kaolinite may undergo a phase transition at ~1572 K, a highest temperature of 700 K was chosen to avoid such structural change. The Young's modulus, strength and elastic constants of kaolinite under various temperatures were calculated, and the relative change of the elastic constant $C_{33}$ with temperature was found to be almost 12 times greater than the relative change of the interlayer constant $C_{11}$. The microstructures under various compressive strains were tracked and they exhibited various failure modes in three directions. The temperature and pressure effects on the mechanical properties of three crystal directions were analysed. The results showed that the Young's modulus of the *z*-direction is the most affected by temperature; however, the influence of temperature on the strengths of the three crystal directions was the same. In addition, the structure of the *z*-direction was the most sensitive to temperature under the same hydrostatic pressure due to the weak interactions between layers.

**Keywords:** kaolinite, mechanical properties, molecular dynamics, pressure and temperature effects

(Received 11 September 2021; revised 9 May 2022; Associate Editor: Hendrik Heinz)

Layered clay minerals such as kaolinite and structurally similar minerals are important in engineering applications (Murray, 2000; Chen *et al*., 2008; Abdi-Khangah *et al*., 2018). The mechanical properties of clay minerals have received significant attention in mining engineering, resource exploration and geotechnical investigations (Wang & Cates, 2001; Szymanska *et al*., 2018; Emmanuel *et al*., 2019). In addition, clay minerals in geological formations can alter seismic-wave propagation, so understanding the mechanical properties of clays helps us to understand, interpret and model the seismic responses of geological structures (Mayoral *et al*., 2016). In recent years, clay minerals have also been used as fillers in polymer nanocomposites, which can improve the strength of materials. For example, Maji *et al*. (2019) prepared polyester polyurethane by incorporating modified and unmodified nanoclays, and they found that the nanocomposites with modified clays provided ~100%, ~135% and ~300% improvements in tensile strength, storage modulus at 25°C and lap shear strength, respectively. Pluart *et al*. (2005) assessed the morphologies and mechanical properties of epoxy clay nanocomposites and observed an improvement in stiffness for exfoliated nanocomposites. In the last few decades, many studies of the mechanical properties of clays and clay minerals have been carried out. For example, Prasad *et al*. (2002) measured the elastic modulus of a dickite sample at nanometre resolution using atomic force microscopy. Vanorio *et al*. (2003) used independent experimental methods to measure the elastic moduli of clay minerals as functions of pressure and saturation. The results they obtained, including the elastic moduli of kaolinite, montmorillonite and smectite, are consistent with reported atomic force acoustic microscopy results on the nanometre scale (Prasad *et al*., 2002).

As a main constituent of layered clay minerals, kaolinite's structure and its physical and chemical properties have been studied for many years. For example, Sato *et al*. (2005) calculated the elastic constant of kaolinite using first-principles calculations. Li *et al*. (2015) investigated the adsorption behaviour and stability of metal ions in defective kaolinite. Compressive strength is one of the major characteristics determining the suitability of clay minerals for particular practical applications, such as metro engineering, tunnel construction, mine-shaft construction and other underground engineering activities (Khan *et al*., 2014). Recently, several works have been carried out on the mechanical behaviour of kaolinite under compression at the atomic scale. For example, Zhang *et al*. (2020) investigated the uniaxial tension and compression of kaolinite using molecular dynamics (MD) simulations. Jia *et al*. (2021) studied the microscopic deformation and crack processes of kaolinite pores under high-pressure water impacts. Several studies have investigated the effects of temperature on the mechanical properties of kaolinite. For example, Yang *et al*. (2019a, 2019b) examined the stress–strain behaviour of kaolinite and defective kaolinite under uniaxial tension at

*Email: qiheng_2000@163.com

**Cite this article:** Cui Y, Wang HY, Zhao HY, Yang H (2022). A molecular dynamics study of the mechanical properties of kaolinite under uniaxial and isothermal compression at various temperatures. *Clay Minerals* **57**, 131–138. https://doi.org/10.1180/clm.2022.21

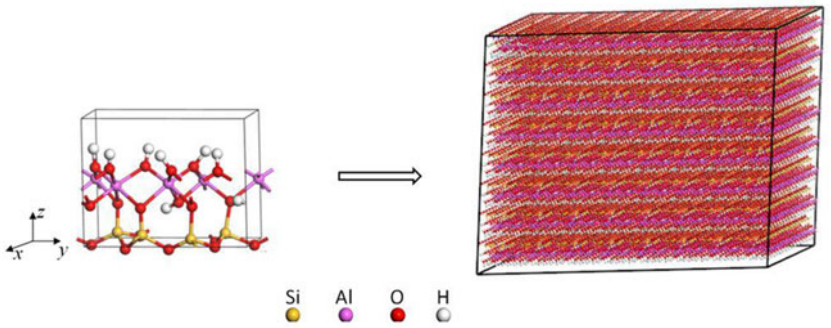


**Fig. 1.** Crystalline structure of kaolinite sheets.

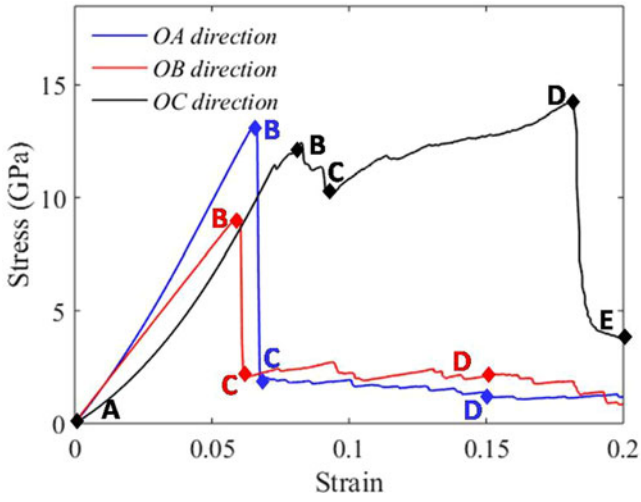


**Fig. 2.** Stress–strain curves of kaolinite when loading along the *x*-, *y*- and *z*-directions. Point A refers to the initial system without strain, and points B, C and D are the strained state at the maximum stress under inflection and after failure, respectively. Point E is the strained state at a strain of 0.2.

various temperatures. Whereas there are multiple studies focusing on the mechanical response of kaolinite as a function of pressure or temperature independent of one another, few studies have been conducted to understand the effects of both temperature and pressure on these mechanical properties. Moreover, previous research has focused on the uniaxial compression behaviour of kaolinite, while the deformation and failure mechanisms under isothermal compression are seldom investigated.

MD simulations represent a well-established method to characterize the properties of materials at the atomic scale, including polymers, nanomaterials, clay minerals, *etc*. For example, Teich-McGoldrick *et al.* (2012) calculated the elastic properties of muscovite under various temperature and pressure conditions using MD simulations. Hantal *et al.* (2014) employed both CLAYFF and REAXFF force fields to investigate the elastic and failure properties of illite, and the results showed that CLAYFF provides a good description of the elastic properties of illite clays, and the stiffness tension determined with CLAYFF can be used to calculate the fracture properties of illite. Benazzouz & Zaoui (2012) determined the superheating temperature of kaolinite to be 1572 K, and they also calculated the elastic constant tensors of kaolinite using MD simulations. In addition, they studied the effects of pressure on the elasticity of kaolinite. Yang *et al.* (2019a, 2019b) simulated the deformation process of and effects of temperature on kaolinite and its defective structure under tension at the atomic scale.

This paper focuses on the deformation and fracture processes of pure kaolinite crystals under uniaxial and isothermal compressions at the atomic scale. Using MD simulations, we obtain the stress–strain curve of kaolinite and clarify its microstructural changes during compression. The mechanical properties of kaolinite under uniaxial and isothermal compression at various temperatures are calculated and discussed. Finally, Young's moduli and strength values obtained using MD simulations are compared with theoretical results.

## Simulation details

The atomic structure of kaolinite is based on the study of Bish (1993). The unit parameters are $a = 5.1535$ Å, $b = 8.9419$ Å, $c = 7.3906$ Å, $\alpha = 9.926°$, $\beta = 105.046°$ and $\gamma = 89.797°$. As is shown in Fig. 1, the layers of kaolinite consist of tetrahedral $SiO_4$ and octahedral $AlO_6$ sheets, and they stack along the *z*-axis. The tetrahedral $SiO_4$ sheets with six-membered silicate rings and the octahedral $AlO_6$ sheets with four-membered aluminate rings are connected by oxygen atoms. In this paper, a periodic supercell of size $16 \times 8 \times 8$ in the *x*-, *y*- and *z*-directions, respectively, was built up by expanding the unit cell. The total number of atoms is 34,816 and the size of initial cell is 82.45 Å × 71.53 Å × 59.12 Å. The initial structure was built using *Materials Studio 7.0* software (Accelrys Software, Inc., CA, USA).

MD simulations were performed using *LAMMPS* software (Plimpton, 1995) developed by Sandia National Laboratories (Albuquerque, NM, USA), and the visualization was realized using *VMD* software (Theoretical and Computational Biophysics Group, IL, USA; Humphrey *et al.*, 1996). The interatomic potential model used here was the CLAYFF force field, which is developed by Cygan *et al.* (2004). The CLAYFF force field can describe the properties of hydroxide, oxyhydroxide and clay phases in non-bonded electrostatic and Lennard–Jones terms. To obtain an equilibrated state, the structure was relaxed for 100 ps under canonical and constant-pressure, constant-temperature ensembles. Uniaxial and isothermal compression were performed using the constant-pressure, constant-temperature ensemble. The uniaxial compression stretched one cell direction uniformly while keeping the other two directions at atmospheric pressure. Hydrostatic pressures between 0.0001 and 50 GPa were applied, and the system was allowed to change volume but not shape. At room temperature, kaolinite has been found to lose long-range crystalline order at >68 GPa; therefore, we restricted our study to pressures below this transition. The confining pressure was also set to be within this range to avoid phase transition. Due to the computational cost and time required to produce results that are qualitatively

https://doi.org/10.1180/clm.2022.21 Published online by Cambridge University Press

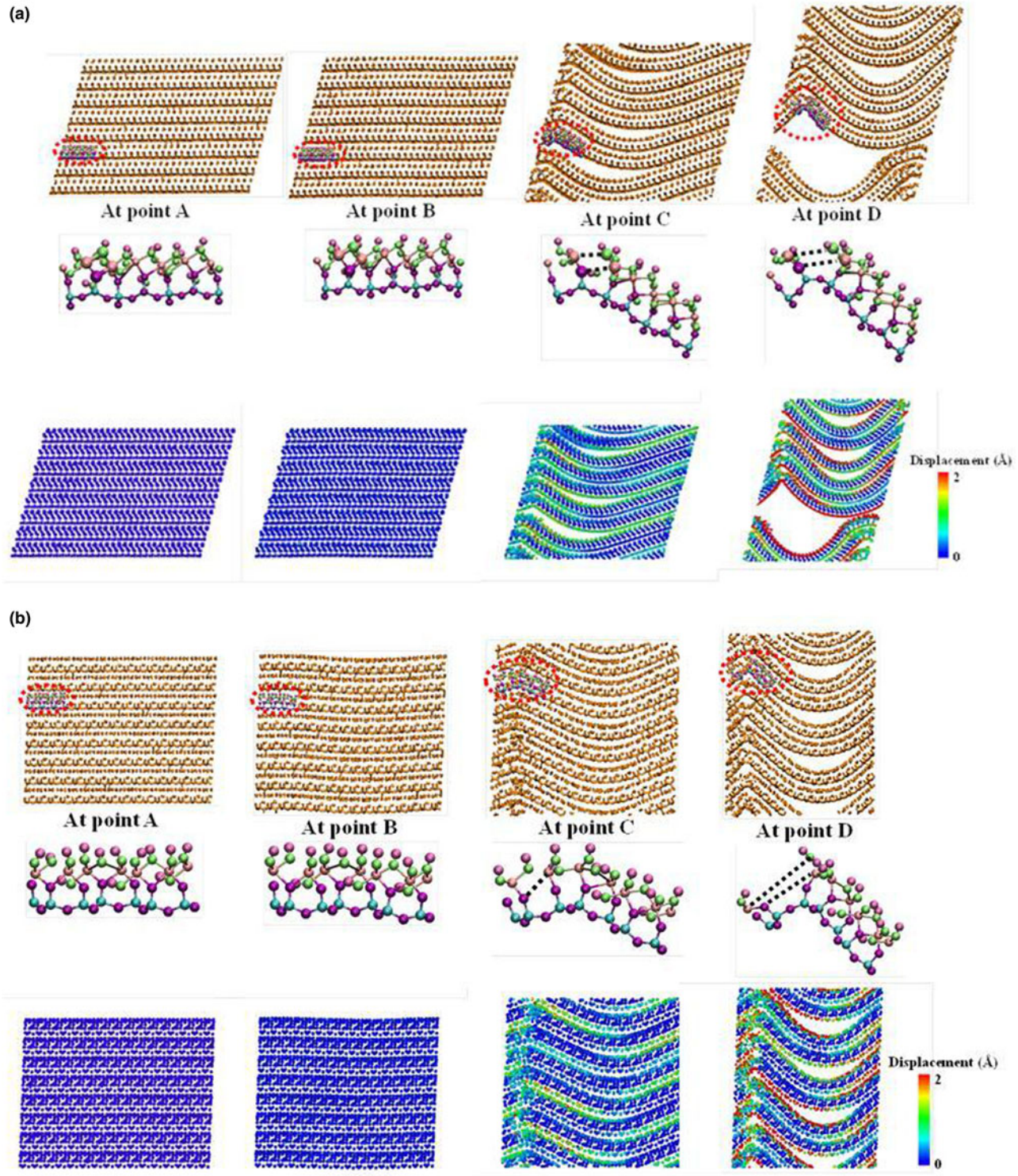


**Fig. 3.** The corresponding microstructures and strain cloud maps at specific points in (a) the *x*-direction, (b) the *y*-direction and (c) the *z*-direction. Please see Fig. 2 for descriptions of points A–E.

similar to experimental results, MD simulations typically use strain rates of ~6–10 orders of magnitude greater than the greatest strain rates often used in experiments (Sahputra & Echtermeyer, 2013). We tested the effects of strain rate on mechanical behaviour using three different strain rates ($5 \times 10^8$, $5 \times 10^9$ and $5 \times 10^{10}$ $s^{-1}$). We found negligible changes in the results as a function of strain rate. To reduce computation time and obtain sufficient configurations under various strain rates, one cell direction was deformed continuously at a strain rate of $5 \times 10^9$ $s^{-1}$. A timestep of 1 fs and a van der Waals cut-off of 10.0 Å were employed in all

https://doi.org/10.1180/clm.2022.21 Published online by Cambridge University Press

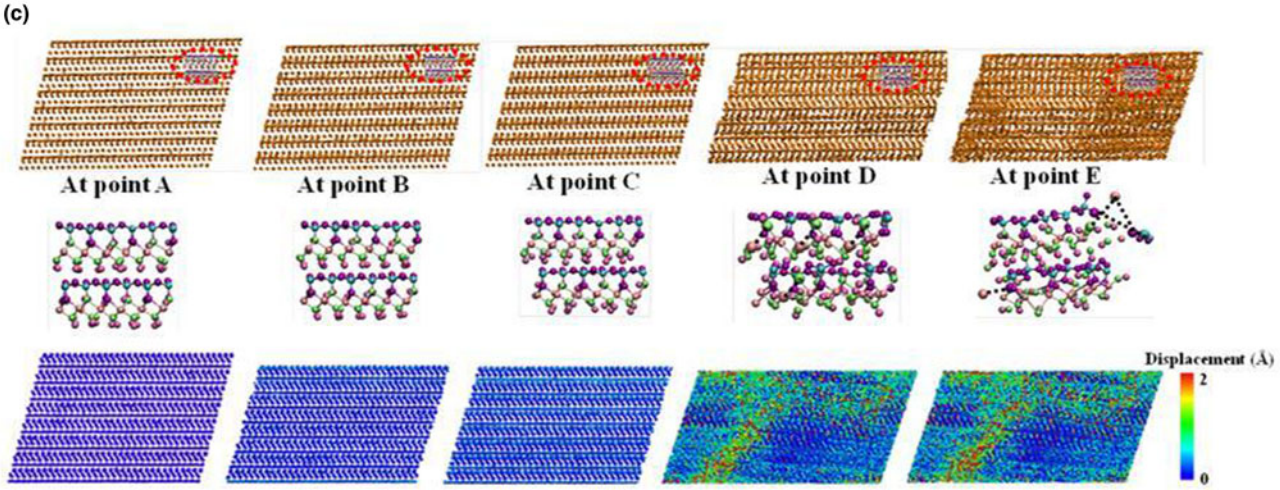


**Fig. 3.** Continued.

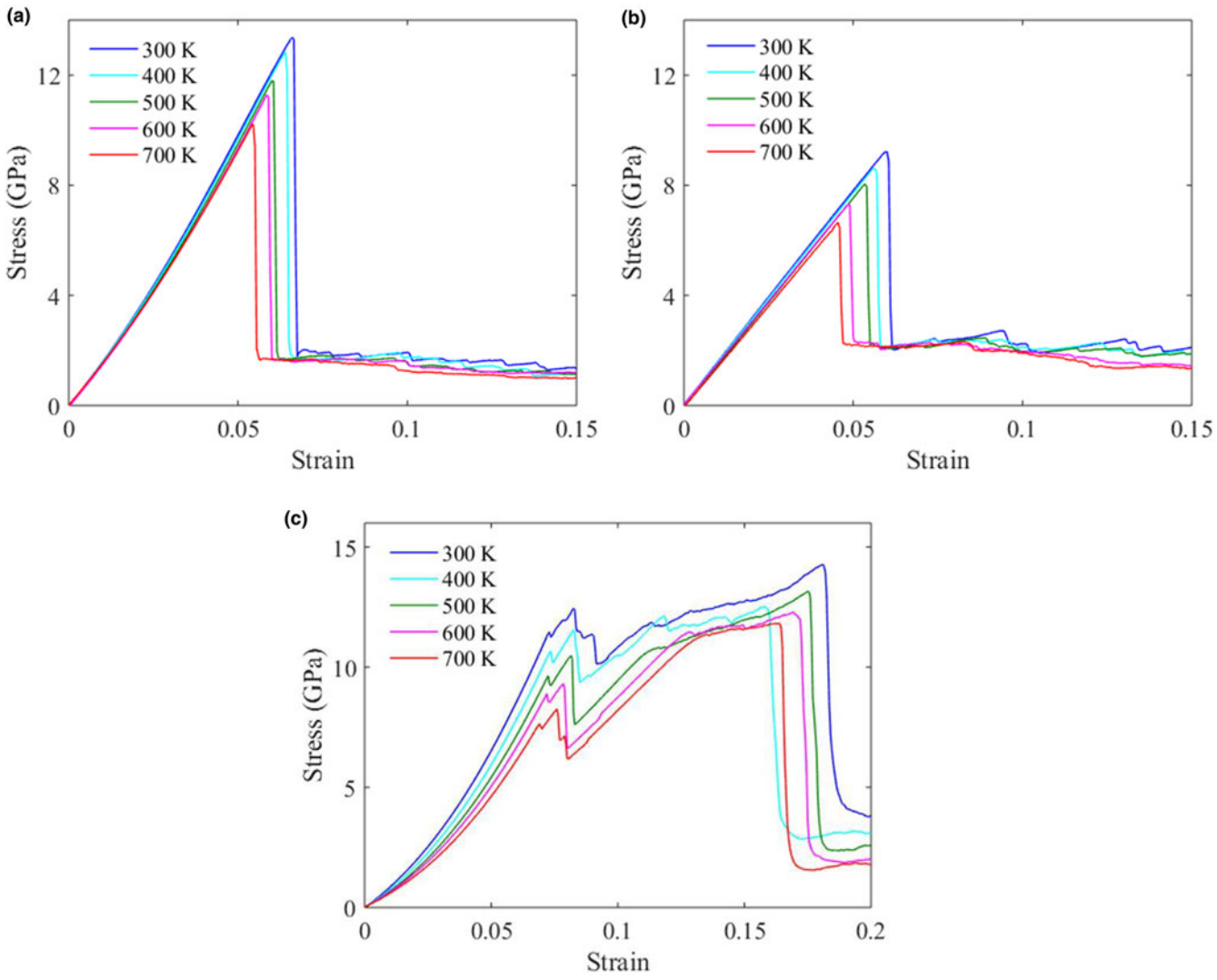


**Fig. 4.** Stress–strain curves of kaolinite at various temperatures when loading along (a) the *x*-direction, (b) the *y*-direction and (c) the *z*-direction.

https://doi.org/10.1180/clm.2022.21 Published online by Cambridge University Press

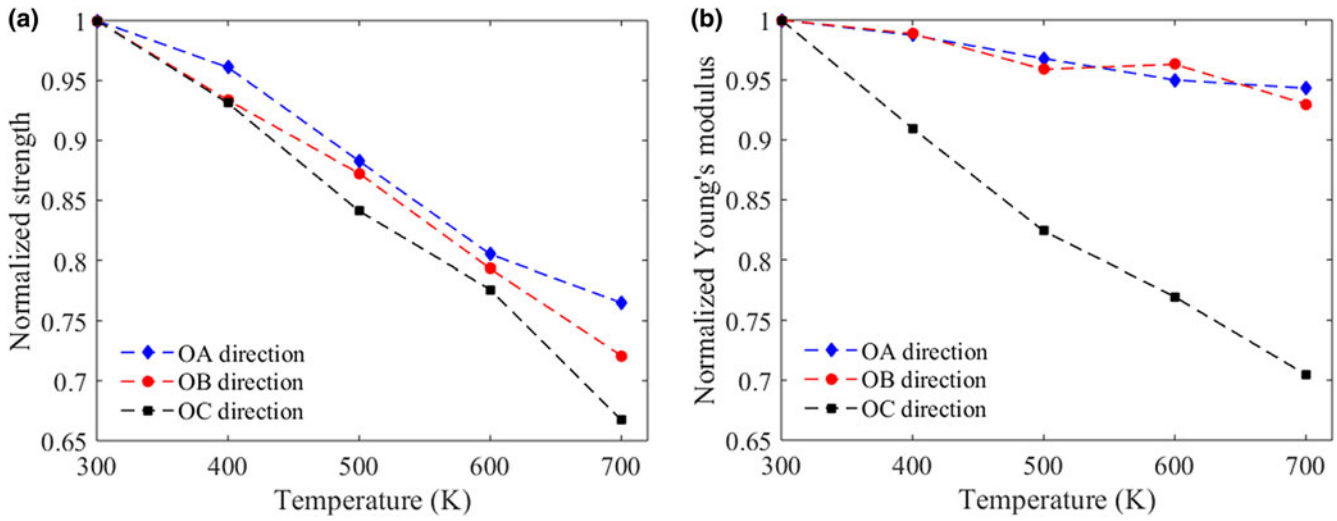


**Fig. 5.** Normalized (a) strength values and (b) Young's moduli of kaolinite in three directions at various temperatures.

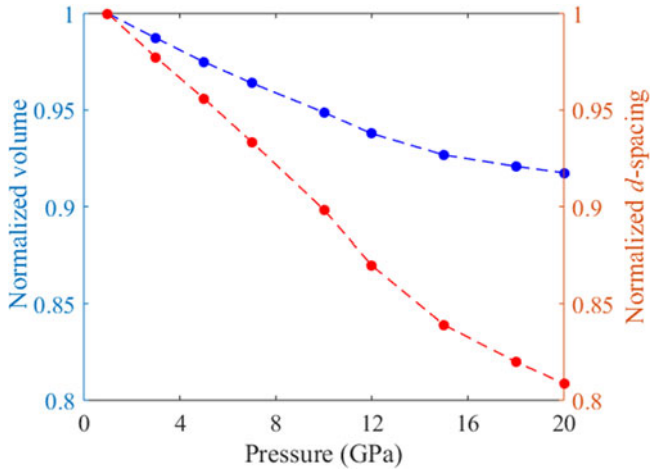


**Fig. 6.** Normalized volume and *d*-spacing of kaolinite at various hydrostatic pressures.

simulations. The Nose–Hoover thermostat and barostat were used for temperature and pressure control, respectively (Hoover, 1985; Allen & Tildesley, 1987).

## Results and discussion

### *Uniaxial compression*

The MD simulations of uniaxial compression tests were carried out by increasing the length of the simulation box continuously along each direction and maintaining a constant volume. The typical stress–strain curves along *x*-, *y*- and *z*-directions are shown in Fig. 2. Periodical boundary conditions are applied in the three directions. The corresponding micro-configurations of kaolinite at these points are shown in Fig. 3, indicating that the structure of kaolinite remains crystalline before reaching the maximum stress. All compressions along different directions produced an elastic response before fracture. However, after the elastic stage, failure modes such as bond breakage and voids together with crack propagation were observed in the molecular structures. Figure 3 shows that, in the *x*- and *y*-directions, the buckling of layers was observed first, then layer separation together with bond breakage took place, which led to sharp reductions in stress according to the stress–strain curves. In the case of loading along the *z*-direction, the gap between layers disappeared first, then layers stacked together, which result in increasing stress according to the stress–strain curves. Finally, bonds were broken with continuing compression. The ductile behaviour of kaolinite in the *z*-direction is a result of the layer spacing between the cation surface of the tetrahedral sheets and the cation surface of the octahedral sheets. The stretching of this layer under load could be the reason for the ductile behaviour of kaolinite in the *z*-direction.

The stress–strain behaviours of kaolinite under uniaxial compression and at various temperatures are shown in Fig. 4. The temperature effect on the stress–strain curves was consistent along all three directions. The normalized Young's moduli and strength are shown in Fig. 5. The results indicate that with increasing temperature, the Young's modulus and strength both decreased in all directions. In addition, the Young's modulus and strength in the *z*-direction decreased the most, with the Young' s moduli in the *x*- and *y*-directions decreasing by almost the same amount; however, the strength in the *y*-direction decreased to a slightly greater extent than that in the *x*-direction. Thus, temperature affected the *z*-direction the most in terms of mechanical properties. In addition, the ultimate strength and fracture strain decreased with increasing temperature. The residual stress remained almost the same at the various temperatures studied.

### *Isothermal compression*

Kaolinite was subjected to hydrostatic compressive stresses ranging from 0.0001 to 50 GPa, and the structural changes and stress–strain relationships are shown in Figs 6 & 7, respectively. The volume and *d*-spacing both decreased with increasing hydrostatic pressure. For all temperatures, the compressive response was almost linear in the *x*- and *y*-directions. However, the curves in Fig. 7c exhibit a parabolic shape in the *z*-direction. Moreover, the hydrostatic pressure had a greater effect in the *z*-direction, as the compressive strain in the *z*-direction was greater by at

https://doi.org/10.1180/clm.2022.21 Published online by Cambridge University Press

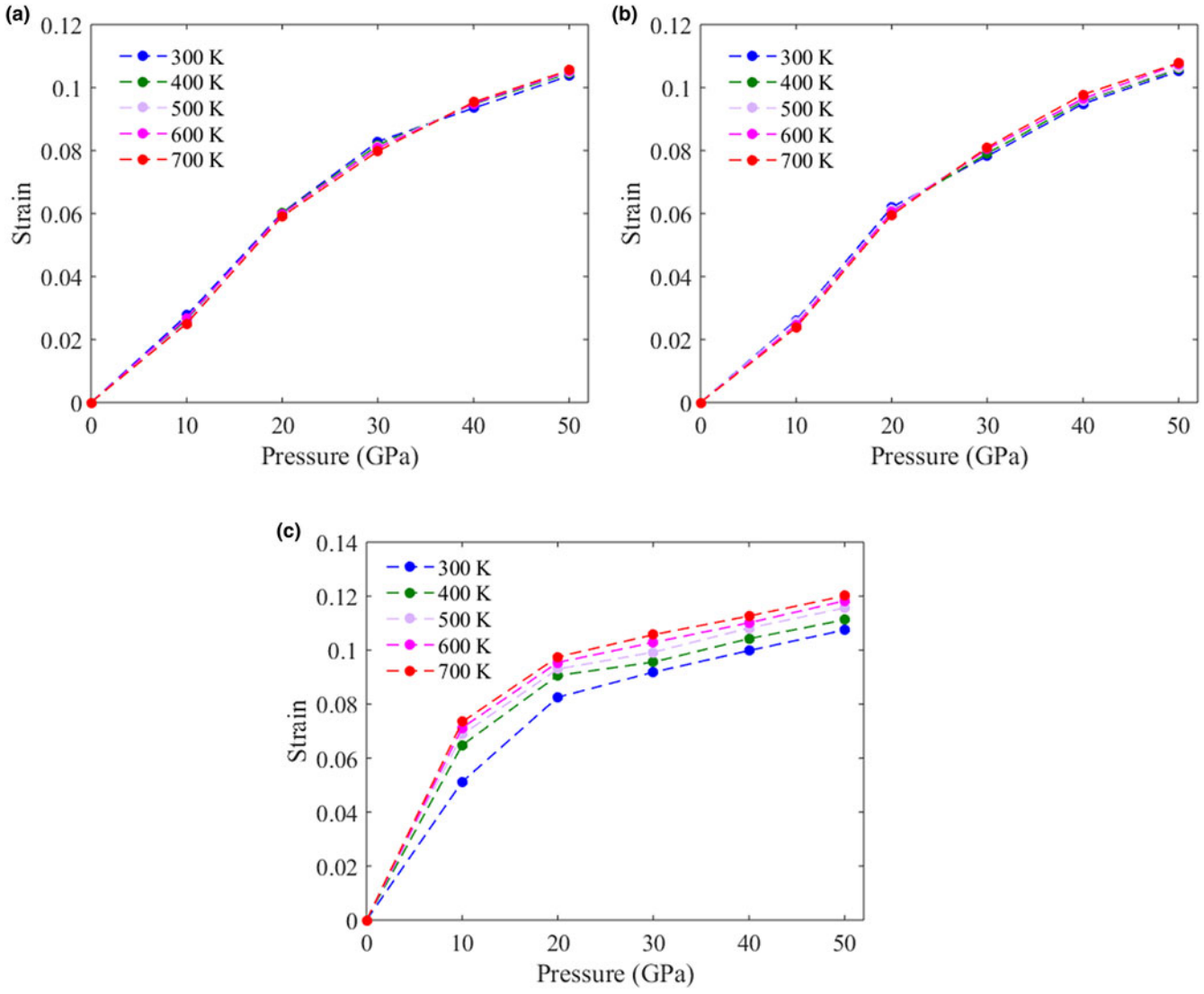


**Fig. 7.** Strain responses of kaolinite at various temperatures in (a) the *x*-direction, (b) the *y*-direction and (c) the *z*-direction as a function of hydrostatic, compressive pressure.

least 50% than in either the *x*- or *y*-directions for the same hydrostatic pressure. The anisotropy of the stress–strain relationship was consistent with the various arrangements of atoms in the lattice.

As is shown in Fig. 7, the effects of temperature on the mechanical properties in the *x*- and *y*-directions were minimal; however, at a given hydrostatic pressure, the compressive strain increased with increasing temperature in the *z*-direction. The radial distribution functions (RDFs) of Al–O bonds under 0 and 30 GPa hydrostatic pressure were calculated at various temperatures, and the results are shown in Fig. 8. With increasing temperature, the values of first peak decreased, indicating the thermal expansion of the kaolinite structure. However, the distance between atom pairs decreased when the pressure increased, indicating that atoms draw closer to each other at greater hydrostatic pressures. The RDF tendencies of Si–O atom pairs at various temperatures and hydrostatic pressures were the same those of Al–O atom pairs.

### *Elastic properties at various temperatures*

The elastic constants are represented by the second derivative of energy density with respect to strain as in Equation 1:

$$C_{ij} = \frac{1}{V}\left(\frac{\partial^2 U}{\partial \varepsilon_i \partial \varepsilon_j}\right) \quad (1)$$

where $V$ is the volume, $U$ is the energy and $\varepsilon$ is the displacement.

Therefore, the elastic constant tensor is a $6 \times 6$ symmetrical matrix. The 21 potentially independent matrix elements are often reduced considerably by symmetry, as is shown by Equations 2 & 3:

$$C_{ij} = \frac{1}{V}\left(D_{\varepsilon\varepsilon} - D_{\varepsilon i} D_{ij}^{-1} D_{j\varepsilon}\right) \quad (2)$$

https://doi.org/10.1180/clm.2022.21 Published online by Cambridge University Press

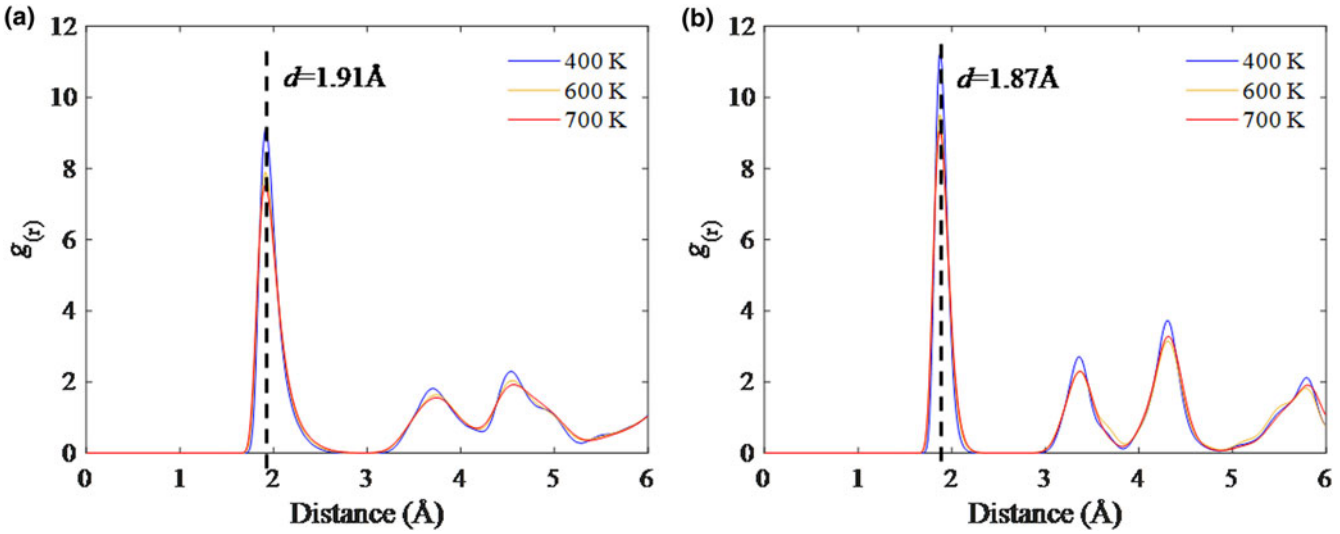


**Fig. 8.** RDFs derived from MD simulations of Al–O bonds for (a) 0.0001 GPa and (b) 30 GPa at various temperatures. $g(r)$ denotes the radial distribution function.

**Table 1.** Elastic constants of kaolinite calculated at various temperatures.

| Elastic constant | 300 K | 500 K | 700 K | Theoretical (300 K)[a] | Experimental (300 K) |
|---|---|---|---|---|---|
| $C_{11}$ | 191.51 | 189.79 | 189.13 | 178.5 ± 8.8 | 171.51[b], 48.1[c], 79.3[c], 121.1[c], 126.4[d] |
| $C_{22}$ | 202.34 | 193.10 | 186.91 | 200.9 ± 12.8 | |
| $C_{33}$ | 74.58 | 58.61 | 46.23 | 32.1 ± 2.0 | 52.62[b], 45.2[c], 72.5[c], 112.5[c], 57.8[d] |
| $C_{44}$ | 6.53 | 5.99 | 5.33 | 11.2 ± 5.6 | 14.76[b], 16.77[c], 25.6[c], 414.1[c], 31.6[d] |
| $C_{55}$ | 8.75 | 6.55 | 2.87 | 22.2 ± 1.4 | |
| $C_{66}$ | 59.08 | 57.07 | 55.16 | 60.1 ± 3.2 | 66.31[b], 16.9[c], 16.3[c], 41.3[c], 53.6[d] |
| $C_{12}$ | 94.25 | 91.64 | 86.78 | 71.5 ± 7.1 | 27.11[b], 12.9[c], 24.1[c], 34.8[c], 8.5[d] |
| $C_{13}$ | 3.97 | 5.03 | 4.83 | 2.0 ± 5.3 | |
| $C_{14}$ | 0.20 | 1.31 | 2.22 | −0.4 ± 2.1 | |
| $C_{15}$ | 2.47 | 1.22 | 1.42 | −41.7 ± 1.4 | |
| $C_{16}$ | −2.37 | −3.11 | −3.60 | −2.3 ± 1.7 | |
| $C_{23}$ | 5.60 | 4.94 | 1.90 | −2.9 ± 5.7 | |
| $C_{24}$ | 2.51 | 2.63 | −0.47 | −2.8 ± 2.7 | |
| $C_{25}$ | 0.71 | −0.02 | −2.94 | −19.8 ± 0.6 | |
| $C_{26}$ | 8.01 | 3.33 | 2.93 | 1.9 ± 1.5 | |
| $C_{34}$ | −0.87 | 0.63 | −1.88 | −0.2 ± 1.4 | |
| $C_{35}$ | −0.52 | −0.60 | −1.48 | 1.7 ± 1.8 | |
| $C_{36}$ | 4.96 | 1.36 | 1.43 | 3.4 ± 2.2 | |
| $C_{45}$ | −0.23 | 0.07 | −2.20 | −1.2 ± 1.2 | |
| $C_{46}$ | −0.91 | −0.43 | −1.26 | 12.9 ± 2.4 | |
| $C_{56}$ | 1.15 | −0.54 | −0.61 | 0.8 ± 0.7 | |

[a]Sato *et al.* (2005).
[b]Katahara (1996).
[c]Wenk *et al.* (2007).
[d]Wenk *et al.* (2008).

where

$$D_{\varepsilon\varepsilon} = \left(\frac{\partial^2 U}{\partial\varepsilon\partial\varepsilon}\right)_{internal},\ D_{\varepsilon i} = \left(\frac{\partial^2 U}{\partial\varepsilon\partial\alpha_i}\right)_{\varepsilon},\ D_{ij} = \left(\frac{\partial^2 U}{\partial\alpha_i\partial\beta_j}\right)_{\varepsilon} \quad (3)$$

The calculated elastic constants of kaolinite are compared in Table 1 with experimental measurements and previous theoretical studies based on density functional theory calculations. As is shown in Table 1, the relative change of the elastic constant $C_{33}$ (describing the interlayer interaction) with temperature was almost 12 times greater than the relative change of the intralayer constant $C_{11}$. In other words, as with the case of the pressure dependence of the elastic constants, the anharmonicity of the bonding forces between the layers was much greater than that of the intralayer forces. Furthermore, the contribution of thermal expansion to this change was much greater for the interlayer elastic constant $C_{33}$ than for the interlayer constant.

## Conclusions

Atomic-scale simulations were conducted to investigate the uniaxial and isothermal compressions of kaolinite under various temperatures. The results indicated that the Young's moduli of kaolinite under uniaxial and isothermal compressions show decreases with increasing temperature, and the $z$-direction was affected the most. In addition, the structure of the $z$-direction is the most sensitive to temperature under the same hydrostatic pressure conditions. Finally, the elastic constants were calculated, and they exhibited decreases with increasing temperature, which is due to the thermal expansion of kaolinite.

**Financial support.** This work was supported by the National Key Research and Development Program of China (2016YFC0600901).

## References

Abdi-Khangah M., Barati H. & Zhang Z (2018) Stability analysis of xanthan–Cr(III)–clay nanocomposite gel: an experimental investigation. *Energy & Fuels*, **32**, 2640–2640.

Allen M.P. & Tildesley D.J. (1987) *Computer Simulation of Liquids*. Oxford University Press, Oxford, UK, 385 pp.

Benazzouz B.K. & Zaoui, A. (2012) A nanoscale simulation study of the elastic behavior in kaolinite clay under pressure. *Materials Chemistry and Physics*, **132**, 880–888.

Bish D.L. (1993) Rietveld refinement of the kaolinite structure at 1.5 K. *Clays and Clay Minerals*, **41**, 738–744.

Chen B., Evans J.R., Greenwell H.C., Boulet P., Coveney P.V., Bowden A.A. & Whiting A. (2008) A critical appraisal of polymer–clay nanocomposites. *Chemical Society Reviews*, **37**, 568–594.

https://doi.org/10.1180/clm.2022.21 Published online by Cambridge University Press

Cygan R.T., Liang J.J. & Kalinichev A.G. (2004) Molecular models of hydroxide, oxyhydroxide, and clay phases and the development of a general force field. *Journal of Physical Chemistry B*, **108**, 1255–1266.

Emmanuel E., Lau C.C., Anggraini V. & Pasbakhsh, P. (2019) Stabilization of a soft marine clay using halloysite nanotubes: a multi-scale approach. *Applied Clay Science*, **173**, 65–78.

Hantal G., Brochard L., Laubie H., Ebrahimi D., Pellenq R.J.M., Ulm F.J. & Coasne B. (2014) Atomic-scale modelling of elastic and failure properties of clays. *Molecular Physics*, **112**, 1294–1305.

Hoover W.G. (1985) Canonical dynamics: equilibrium phase-space distributions. *Physical Review A*, **31**, 1695–1697.

Humphrey W., Dalke A. & Schulten K. (1996) *VMD* – visual molecular dynamics. *Journal of Molecular Graphics*, **14**, 33–38.

Jia X.T., Hao Y.Z., Li P.C., Zhang X. & Lu D.T. (2021) Nanoscale deformation and crack processes of kaolinite under water impact using molecular dynamics simulations. *Applied Clay Science*, **206**, 106071.

Katahara K.W. (1996) Clay mineral elastic properties. *SEG Technical Program Expanded Abstracts*, **1996**, 1691–1694.

Khan F.S., Azam S., Rahunandan M.E. & Clark R. (2014) Compressive strength of compacted clay–sand mixes. *Advances in Materials Science and Engineering*, **2014**, 921815.

Li X., Li H. & Yang G. (2015) Promoting the adsorption of metal ions on kaolinite by defect sites: a molecular dynamics study. *Scientific Reports*, **5**, 14377.

Mayoral J.M., Castanon E., Alcantara L. & Tepalcapa S. (2016) Seismic response characterization of high plasticity clays. *Soil Dynamics and Earthquake Engineering*, **84**, 174–189.

Murray H.H. (2000) Traditional and new applications for kaolin, smectite, and palygorskite: a general overview. *Applied Clay Science*, **17**, 207–221.

Plimpton S. (1995) Fast parallel algorithms for short-range molecular-dynamics. *Journal of Computational Physics*, **117**, 1–19.

Pluart L., Duchet J. & Sautereau H. (2005) Epoxy/montmorillonite nanocomposites: influence of organophilic treatment on reactivity, morphology and fracture properties. *Polymer*, **46**, 12267–12278.

Prasad M., Kopycinska M., Rabe U. & Arnold W. (2002) Measurement of Young's modulus of clay minerals using atomic force acoustic microscopy. *Geophysical Research Letters*, **29**, 1172.

Sahputra I.H. & Echtermeyer A.T. (2013) Effects of temperature and strain rate on the deformation of amorphous polyethylene: a comparison between molecular dynamics simulations and experimental results. *Modelling and Simulation in Materials Science and Engineering*, **21**, 065016.

Sato H., Ono K., Johnston C.T. & Yamagishi A. (2005) First-principles studies on the elastic constants of a 1:1 layered kaolinite mineral. *American Mineralogist*, **90**, 1824–1826.

Szymanska J., Wisniewski P., Wawulska-Marek P. & Mizera J. (2018) Determination of loamy resources impact on granulation of ceramic proppants and their properties. *Applied Clay Science*, **166**, 327–338.

Teich-McGoldrick S.L., Greathouse J.A. & Cygan R.T. (2012) Molecular dynamics simulations of structural and mechanical properties of muscovite: pressure and temperature effects. *Journal of Physical Chemistry C*, **116**, 22–45.

Vanorio T., Prasad M. & Nur A. (2003) Elastic properties of dry clay mineral aggregates, suspensions and sandstones. *Geophysical Journal International*, **155**, 319–326.

Wang H. & Cates M.E. (2001) Effective elastic properties of solid clays. *Geophysics*, **66**, 428–440.

Wenk H.R., Lonardelli I. & Ren Y. (2007) Preferred orientation and elastic anisotropy of illite-rich shale. *Geophysics*, **72**, 69–75.

Wenk H.R., Voltolini M., Mazurek M., Van Loon L.R. & Vinsot A. (2008) Preferred orientations and anisotropy in shales: Callovo-Oxfordian shale (France) and Opalinus Clay (Switzerland). *Clays and Clay Minerals*, **56**, 285–306.

Yang H., Han Z.F. & He M.C. (2019a) Defect and temperature effects on mechanical properties of kaolinite: a molecular dynamics study. *Clay Minerals*, **54**, 154–159.

Yang H., He M.C., Lu C.S. & Gong W.L. (2019b) Deformation and failure processes of kaolinite under tension: insights from molecular dynamics simulations. *Science China Physics, Mechanics & Astronomy*, **62**, 64612.

Zhang L.L., Zheng Y.Y., Wei P.C., Diao Q.F. & Yin Z.Y. (2020) Nanoscale mechanical behavior of kaolinite under uniaxial strain conditions. *Applied Clay Science*, **201**, 105961.

https://doi.org/10.1180/clm.2022.21 Published online by Cambridge University Press